# Solvation Dynamics in Reverse Micelles: The Role of Headgroup−Solute Interactions[†]

## James Faeder[‡] and Branka M. Ladanyi*,[§]

*Theoretical Biology and Biophysics Group, MS K710, Los Alamos National Laboratory,
Los Alamos, New Mexico 87545, and Department of Chemistry, Colorado State University,
Fort Collins, Colorado 80523*

We present molecular dynamics simulation results for solvation dynamics in the water pool of anionic-surfactant reverse micelles (RMs) of varying water content, $w_0$. The model RMs are designed to represent water/aerosol-OT/oil systems, where aerosol-OT is the common name for sodium bis(2-ethylhexyl)sulfosuccinate. To determine the effects of chromophore−headgroup interactions on solvation dynamics, we compare the results for charge localization in model ionic diatomic chromophores that differ only in charge sign. Electronic excitation in both cases is modeled as charge localization on one of the solute sites. We find dramatic differences in the solvation responses for anionic and cationic chromophores. Solvation dynamics for the cationic chromophore are considerably slower and more strongly $w_0$-dependent than those for the anionic chromophore. Further analysis indicates that the difference in the responses can be ascribed in part to the different initial locations of the two chromophores relative to the surfactant interface. In addition, slow motion of the cationic chromophore relative to the interface is the main contributor to the longer-time decay of the solvation response to charge localization in this case.

## I. Introduction

Solvent-induced shifts in absorption and emission spectra of chromophores provide valuable information on the solvation properties, such as the local polarity, of condensed-phase media.[1] The time evolution of the Stokes shift of the fluorescence spectra provides additional information on the time scale of local structural rearrangements that occur in response to changes in solute electronic structure.[2−7] The solvation time evolution of the solvation response is usually quantified in terms of $S(t)$, given by[5,7]

$$S(t) = \frac{\nu_{max}(t) - \nu_{max}(\infty)}{\nu_{max}(0) - \nu_{max}(\infty)} \qquad (1)$$

where $\nu_{max}$ is the peak frequency of the fluorescence spectrum, $t$ is the time after excitation, which occurs at $t = 0$, and $\nu_{max}(\infty)$ denotes the steady-state emission-peak frequency.

The mechanism of solvation dynamics in bulk polar liquids is now quite well understood. $S(t)$ in response to a change in solute charge distribution decays largely through collective reorientation[8−10] and is reasonably well-predicted from the solvent dielectric permittivity.[5,11−13]

In heterogeneous solvent environments, such as surfactant self-assemblies and other systems containing liquid interfaces, the location of the chromophore relative to the interface can strongly affect its electronic spectra.[14−25] In the case of solvation dynamics, a change in the solute location relative to the interface might be required in order to attain the free energy minimum for the solvation of the excited-state charge distribution. Several computer simulations of solvation dynamics in systems contain-ing interfaces of liquids with other phases have shown that these additional mechanisms can make significant contributions to the Stokes shift relaxation.[22,23,26,27]

In this work, we examine the effects of system heterogeneity on solvation dynamics in reverse micelles (RMs). In RMs, a surfactant encloses nanoscopic, approximately spherical droplets of a polar liquid, usually water, within a continuous nonpolar phase. RMs serve as models for biological membranes and have numerous practical applications including as media for heterogeneous chemical and biochemical catalysis, drug delivery, and nanoparticle synthesis.[28−31] In many of the RM applications, the fact that the size of the water droplet can be controlled simply by changing the molar ratio of water to surfactant plays an important role. Specifically, for a given nonpolar (oil) phase, the diameter of the approximately spherical polar nanoscopic droplet is proportional to the water content[31−33]

$$w_0 = [H_2O]/[surfactant] \qquad (2)$$

Water-soluble chromophores partition to the RM interior, and their electronic spectra can serve as probes of the confined aqueous environment.[16,34] Measurement of solvation dynamics involving such chromophores has been an active area of research in recent years.[18,35−51] While results with time resolution comparable to that reported for bulk water[52,53] are not yet available, it is clear that the environment probed differs substantially from bulk water. Specifically, the solvation response $S(t)$ has appreciable contributions from slowly decaying processes,[38,39,42,45,46,54] some on time scales considerably slower than the water reorientation rate measured by NMR.[55] The decay rates for a given chromophore are usually $w_0$-dependent,[38,44,46] with slower relaxation observed at smaller $w_0$, as might be expected in view of the stronger confinement and the tighter packing of the surfactant headgroups at the interface.[32] In a given RM system, different chromophores sometimes give rise to very

---

Solvation Dynamics in Reverse Micelles

*J. Phys. Chem. B, Vol. 109, No. 14, 2005* **6733**

different $S(t)$ values,[35] signaling that a different mix of the available mechanisms and solvent environments is sampled in the course of the solvation event. Computer simulation can provide insights into this and other effects of medium heterogeneity on the solvation dynamics, given that the time evolution of the solute location can be followed in addition to obtaining $S(t)$.

We have previously carried out a molecular dynamics (MD) simulation study of solvation dynamics in model RMs designed to represent the water/aerosol-OT (AOT)/oil system, where aerosol-OT is the common name for sodium bis(2-ethylhexyl)-sulfosuccinate, at several values of $w_0$.[56] The model chromophore that we chose for that study was negatively charged and was excluded from the RM interface by strong repulsive interactions with the AOT surfactant $-SO_3^-$ headgroups. The $S(t)$ values that we found were weakly $w_0$-dependent, reflecting the localization of the chromophore in the core of the aqueous droplet, where the solvent mobility was less restricted. We examine here the effects of electrostatic attraction between the chromophore and the headgroup by comparing solvation responses to charge localization in model ionic chromophores that differ only in the sign of their charge. The effect of water pool size is investigated as well by carrying out MD simulations of solvation dynamics in AOT-like RMs in the $w_0$ range 2–7.5.

The remainder of this paper is organized as follows. In section II, we describe our RM and chromophore models and provide the details of our MD simulations. In section III, we describe the theoretical background for modeling solvation dynamics in multicomponent systems. Our results are presented in section IV, starting with the chromophore location in the RM, proceeding to $S(t)$ and then to analysis of nonequilibrium trajectories to determine mechanistic details of the solvation response. A summary and conclusions are presented in section V.

## II. Model and Computational Details

The present simulations are based on a reverse micelle model that we have developed previously[57] and applied to solvation dynamics of charge localization within a diatomic chromophore resembling $I_2^-$.[56] Briefly, the model is based on a near-atomistic representation of the RM interior region and on a nonpolar continuum representation of the surfactant tails and the nonpolar phase. The RMs are designed to be models for water-in-oil microemulsions in which the oil phase is isooctane and the surfactant aerosol-OT (AOT), which has a sulfonate headgroup and $Na^+$ counterion. Thus, the RM water pool radii $R$ for particular $w_0$ values were chosen to correspond to those estimated based on light scattering results for this system.[32] In the presence of the chromophore, the $R$ values were increased slightly to accommodate one chromophore molecule per RM without a significant increase in pressure.[56] The species in the RM interior (water, surfactant headgroups, counterions, and the chromophore) are assumed to interact via a site–site Lennard-Jones (LJ) + Coulomb potential with Lorentz–Berthelot combining rules.[58] A single-site representation of the sulfonate headgroup ($Z^-$) is adopted. The nonpolar portion of the system is represented as a spherical cavity of radius $R$ with LJ parameters appropriate for hydrocarbons,[59] averaged over a spherical surface.[57] The headgroups are attached to the interface in the radial direction by a harmonic spring, with the force constant in the range of values corresponding to covalent bonding. Water is represented by the SPC/E model,[60] and the $Na^+$ parameters are taken from a simulation of sodium dodecyl sulfate surfactant.[61] The LJ potential parameters and partial charges of all species as well as other input parameters into the

**TABLE 1: Intermolecular Potential and Molecular Parameters**

| A. Intermolecular Potential | | | |
|---|---|---|---|
| site | $\epsilon_\alpha/k$ (K) | $\sigma_\alpha$ (Å) | $q_\alpha$ (e) |
| H | 0 | – | 0.4238 |
| O | 78.24 | 3.166 | −0.8476 |
| $Na^+$ | 58.01 | 2.275 | 1.0 |
| $Z^-$ | 251.58 | 6.000 | −1.0 |
| $Cl^-$ | 50.30 | 4.504 | −1.0 |
| I(1) | 169.50 | 3.610 | $\pm 0.5(\pm 1.0)^a$ |
| I(2) | 169.50 | 3.610 | $\pm 0.5(0.0)^a$ |
| wall[b] | 231.55 | 2.500 | 0 |

| B. Molecular Structure and Harmonic Potential Parameters | |
|---|---|
| water | $R_{OH} = 1.00$ Å |
| | $\angle_{HOH} = 109.5°$ |
| "$I_2^+$", $I_2^-$ | $R_{II} = 3.23$ Å |
| headgroup–wall | $d_e = 2.50$ Å |
| harmonic potential | $k_e = 600$ kcal mol$^{-1}$ Å$^{-1}$ |

$^a$ Excited-state charges in parentheses. The positive charges are for "$I_2^+$", the negative for $I_2^-$. $^b$ The functional form appropriate for a spherical cavity is given in ref 57.

interaction model are summarized in Table 1. Readers are referred to ref 57 for additional model and simulation details.

Atomistic simulations of aqueous RMs, in which all components are explicitly modeled, have recently been performed.[62−68] Senapati and Berkowitz studied water structure and dynamics in fluorosurfactant-based reverse micelles.[66] Incorporating a newly developed algorithm to account for the effect of the roughness of the surfactant–water interface,[69] they were able to demonstrate the layering of water in the interfacial region that was previously observed in simulations of RMs with fixed cavities,[57] but which is obscured in the standard density profiles. In addition to reducing the time required to compute the molecular dynamics, the fixed-cavity model we use here greatly simplifies the analysis of the interfacial structure in comparison with all-atom simulations. It is also worth noting that the cavity model has recently been shown to accurately reproduce the key features of interfacial water structure and dynamics probed experimentally by quasi-elastic neutron scattering.[70]

To determine the effects of solute–headgroup electrostatic interactions on solvation dynamics, the two model chromophores that we consider differ only in the signs of the site charges. Thus the results obtained previously for a chromophore with LJ parameters and bond length corresponding to a rigid version of the $I_2^-$ ion[71] are compared to the results for a diatomic ion that differs from it only in the charge sign. We denote this ion as "$I_2^+$". Both chromophores are simpler than the aqueous solvation dynamics probes used in experiments. We have chosen simple solute models in order to facilitate identification of the key steps in the solvation mechanism. In future studies, we plan to make a closer contact with experiments by carrying out simulations using atomistic models of chromophores, such as coumarin 343 (C343),[13,27,72] used in experiments on solvation dynamics in RMs.

Table 2 contains information on the compositions and sizes of RMs with either $I_2^-$ or "$I_2^+$" chromophores for $w_0 = 2, 4$, and 7.5. Note that the systems are electrically neutral. In the case of the RMs containing the "$I_2^+$" chromophore, a $Cl^-$ ion serves to balance its charge, while in RMs containing $I_2^-$ an extra $Na^+$ ion provides charge balance. The $Cl^-$ LJ parameters are taken from ref 73.

As in our previous MD study of solvation dynamics in RMs,[56] chromophore electronic excitation is modeled as charge local-

**TABLE 2: Reverse Micelle Parameters**

| | | | "$I_2^+$" Reverse Micelles | | | |
|---|---|---|---|---|---|---|
| $w_0$ | $n$ (H$_2$O) | $n$ (Na$^+$) | $n$ (Z$^-$) | $n$ (I$_2^+$) | $n$ (Cl$^-$) | $R$ (Å) |
| 2 | 52 | 26 | 26 | 1 | 1 | 11.74 |
| 4 | 140 | 35 | 35 | 1 | 1 | 14.08 |
| 7.5 | 525 | 70 | 70 | 1 | 1 | 19.41 |

| | | | I$_2^-$ Reverse Micelles | | | |
|---|---|---|---|---|---|---|
| $w_0$ | $n$ (H$_2$O) | $n$ (Na$^+$) | $n$ (Z$^-$) | n (I$_2^-$) | $n$ (Cl$^-$) | $R$ (Å) |
| 2 | 52 | 27 | 26 | 1 | 0 | 11.70 |
| 4 | 140 | 36 | 35 | 1 | 0 | 14.06 |
| 7.5 | 525 | 71 | 70 | 1 | 0 | 19.40 |

**TABLE 3: MD Trajectories for I$_2^+$ Reverse Micelle Production Runs**

| $w_0$ | length of equilibrium GS trajectories (ns) | length of equilibrium ES trajectories (ns) | no. of nonequilibrium trajectories |
|---|---|---|---|
| 2 | 25 | 30 | 600 |
| 4 | 30 | 30 | 600 |
| 7.5 | 10 | 7 | 500 |

ization, which results in a dipole change $0 \rightarrow 7.76$ D. Specifically, for both solutes, the change in solute partial charges resulting from the $S_0 \rightarrow S_1$ transition is $(q/2, q/2) \rightarrow (q, 0)$, where $q = -e$ for I$_2^-$ and $q = e$ for "I$_2^+$." It should be noted that this change in dipole is about 3 times larger than that for C343,[13,27,72] the chromophore used in many experiments on solvation dynamics in aqueous systems. Our model chromophores are also smaller in size.

The MD simulations were carried out with a time step of 2 fs, using the generalized method of constraints to fix the H$_2$O molecule geometry.[74] A Berendsen thermostat[75] with a time constant of 0.4 ps during equilibration and 2 ps during production runs was used to maintain the average temperature at 300 K. Table 3 summarizes the information on the length of MD equilibrium trajectories and numbers of nonequilibrium trajectories.

## III. Simulation of Solvation Dynamics

Solvation dynamics has been a subject of numerous theoretical and experimental studies in the last 15 years, with many of the results obtained for bulk liquids summarized in review articles.[2-7] It refers to the rate of solvent reorganization in response to a change in solute properties brought about by its electronic excitation. As noted in the Introduction, this response is usually reported as $S(t)$, given by eq 1. The time evolution of the Stokes shift is due to the solvent effects on the vertical energy gap between the $S_0$ and $S_1$ solute electronic states. C343 and other chromophores that are used in solvation dynamics experiments are structurally quite rigid, and their structure is weakly perturbed by the $S_0 \rightarrow S_1$ electronic transition, so the main source of the solvent effect is the change $\Delta E$ in the solute$-$solvent potential,[5,7,76]

$$\Delta E = U_1 - U_0 \tag{3}$$

where $U_n$ is the solute$-$solvent potential in the solute electronic state $S_n$. A computationally accessible expression for $S(t)$ is obtained by expressing it in terms of $\overline{\Delta E}$. This is achieved by relating the nonequilibrium average $\overline{\Delta E(t)}$ to the time evolution of $\nu_{max}$

$$h\nu_{max}(t) = \overline{\Delta E(t)} + h\nu_{el} \tag{4}$$

where $\nu_{el}$ is the electronic transition frequency for the isolated solute and the overbar indicates an average over different microscopic solvent environments corresponding to the macroscopic experimental conditions;[76] the solvent is initially equilibrated with the ground-state solute, and the solute$-$solvent potential is instantaneously changed at $t = 0$. Through use of eq 4, the solvation response becomes

$$S(t) = \frac{\overline{\Delta E(t)} - \overline{\Delta E(\infty)}}{\overline{\Delta E(0)} - \overline{\Delta E(\infty)}} \tag{5}$$

Although there may be some changes in the nonelectrostatic portion of the solute$-$solvent potential, which would, for example, lead to a change in the solute LJ parameters,[77,78] most of $\Delta E$ in the case of commonly used chromophores results from the change in the solute charge distribution.[79] In our model chromophores, the LJ portion of the potential does not depend on the electronic state of the chromophore, so $\Delta E$ is purely electrostatic,

$$\Delta E = \sum_{j=1}^{N} \sum_{\alpha \in 0} \sum_{\beta \in j} \frac{\Delta q_{0\alpha} q_{j\beta}}{4\pi\epsilon_0 |\mathbf{r}_{0\alpha} - \mathbf{r}_{j\beta}|} \tag{6}$$

where $j$ denotes the $j$th solvent molecule, $\alpha$ denotes a solute (molecule 0) site, $\beta$ a site on the $j$th solvent molecule, $\Delta q_{0\alpha}$ the change due to electronic excitation in the partial charge of the solute site $\alpha$, $\mathbf{r}_{0\alpha}$ the position of this site, $q_{j\beta}$ the partial charge on site $\beta$ on the $j$th solvent molecule, and $\mathbf{r}_{j\beta}$ the position of this site.

The main goal of this work is to examine how headgroup$-$chromophore electrostatic interactions affect solvation dynamics. We have shown in our previous study of solvation dynamics in RMs that a negatively charged chromophore, chosen as a simple model for the C343 chromophore used in most experiments on solvation dynamics in aqueous media, resides in the core of the RM water pool. Consequently, its $S(t)$ value is dominated by the water response and weakly dependent on RM size. Here, we consider a chromophore of equal and opposite charge, which should have greater probability of residing near the interface due to its attraction to the surfactant headgroups. For both chromophores, electronic excitation is represented as charge localization, which leads to dipole creation in a previously nondipolar molecule.

To simulate solvation dynamics, we have carried out both equilibrium and nonequilibrium MD simulations with solute-containing RMs. Equilibrium trajectories with the solute in the $S_0$ state were used to generate starting configurations, sampled at equal time intervals, for the nonequilibrium trajectories and to compute equilibrium time correlation functions (TCFs). Equilibrium trajectories with the solute in the $S_1$ state were used to determine $\overline{\Delta E(\infty)}$. In the nonequilibrium trajectories, the solute charges were changed instantaneously at $t = 0$ from the $S_0$ to the $S_1$ charge distribution. In the case of "I$_2^+$", each nonequilibrium trajectory was run for 5 ps in order to compute $\overline{\Delta E(t)}$, the time-dependent Stokes shift. The number of nonequilibrium trajectories and the lengths of the equilibrium runs for the systems containing the "I$_2^+$" solute are given in Table 3. The corresponding information for the I$_2^-$ can be found in Table 3 of ref 56.

The equilibrium trajectory data were used to generate the TCFs

$$C_0(t) = \langle \delta\Delta E(0)\delta\Delta E(t) \rangle_0 / \langle [\delta\Delta E]^2 \rangle_0 \tag{7}$$

Solvation Dynamics in Reverse Micelles

*J. Phys. Chem. B, Vol. 109, No. 14, 2005* **6735**

of fluctuations $\delta\Delta E = \Delta E - \langle\Delta E\rangle_0$ in $\Delta E$, where $\langle\cdots\rangle$ denotes an equilibrium ensemble average and the subscript 0 indicates that it was evaluated in the presence of the $S_0$ solute. One can define in an analogous way $C_1(t)$, the TCF of $\delta\Delta E$ in the presence of the $S_1$ solute. Within the stationary linear response approximation,[80] in which the response is assumed independent of the time origin,[81]

$$S(t) \cong C_0(t) \cong C_1(t) \tag{8}$$

Here, we test the approximation $S(t) \cong C_0(t)$ in the case of the "$I_2^+$" solute. We had previously found that the approximation is reasonably good in the case of $I_2^-$, especially for the longer-time response.[56]

Given that the contributions to $\Delta E$ from different species in the RM water pool are additive in our model, as shown by eq 6, we can express $S(t)$ as a sum of such contributions. In the case of the "$I_2^+$" solute,

$$S(t) = S_{H_2O}(t) + S_{Na^+}(t) + S_{Z^-}(t) + S_{Cl^-}(t) \tag{9}$$

while for $I_2^-$ the last term is absent. For a given species $m$, $S_m(t)$ is given by

$$S_m(t) = \frac{\overline{\Delta E_m(t)} - \overline{\Delta E_m(\infty)}}{\overline{\Delta E(0)} - \overline{\Delta E(\infty)}} \tag{10}$$

where $\Delta E_m$ is the contribution to $\Delta E$ from the solute interacting with the component $m$ of the RM water pool.

## IV. Results

**A. Solute Location within the Reverse Micelle.** Figure 1 displays the radial probability densities of solute sites as a function of the radial distance $D$ from the average positions of the headgroups for the ground-state $I_2^-$ and "$I_2^+$" model chromophores, revealing sharp differences in the locations of the two solutes within the RMs. $I_2^-$ is never found in the interfacial region for all $w_0$ values displayed. Its distribution exhibits split peaks, neither one of which is close to $D = 0$, the average location of the headgroups. As $w_0$ increases, the distribution becomes more diffuse, and the peak closer to the interface moves toward the interface. These trends are understandable, given that the core region increases in size and the surface charge density decreases as $w_0$ increases. However, even at $w_0 = 7.5$, the largest RM size displayed, the solute avoids the $D$ range for which contact with the headgroups is possible.

By contrast, for "$I_2^+$", the iodine atom probability density has a peak near $D = 0$ in all three RM sizes, indicating that the solute is likely to be in the interfacial region and between the headgroups. The other sharp peak is in the interfacial region at around $D = 3$ Å, which corresponds to the I−I bond length (Table 1), indicating a prevalent structure in which one of the solute atoms is between the headgroups with the solute bond perpendicular to the interface. The third peak in the "$I_2^+$" atom probability distribution is more diffuse than the first two and occurs at around 4.8 Å, a distance close to the headgroup−iodine atom LJ contact value, indicating solute location just on the inside of the shell occupied by the headgroups.

Figure 2 depicts schematically the locations of the negatively and positively charged chromophores in anionic RMs. We expect that this difference in location relative to the interface will result in differences in the observed solvation dynamics. We also expect that the "$I_2^+$" chromophore will be a more
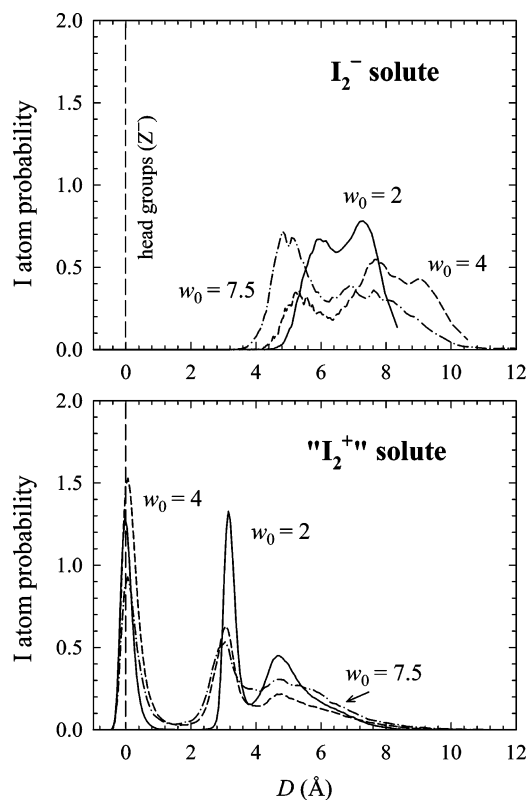


**Figure 1.** Iodine atom probability density for ground-state solutes as a function of the distance $D$ from the average position of the headgroups. The top panel depicts the results for the $I_2^-$, and the bottom panel for the "$I_2^+$" solute. Different line styles indicate the results for different reverse micelle water content $w_0$ (which is proportional to the RM diameter).

sensitive probe of the changes in water mobility with the RM size, because this mobility varies more rapidly near the interface.[57]

**B. Solvation Dynamics.** Figure 3 depicts the results for the solvation response, $S(t)$, in the three RM sizes considered, for charge localization in $I_2^-$ (top panel) and "$I_2^+$" (bottom panel). The solvation dynamics are strikingly different for these two chromophores. In the case of "$I_2^+$", $S(t)$ exhibits strong dependence on RM size, while for $I_2^-$ the RM size dependence is negligible at short times ($t < 0.2$ ps) and quite weak after that. For "$I_2^+$", the amplitude of the slowly decaying component decreases sharply as $w_0$ increases and overall $S(t)$ decays more slowly for "$I_2^+$" than for $I_2^-$ at all sizes studied. As we have shown previously, water mobility is sharply reduced at small values of $w_0$ but increases sharply as $w_0$ is increased.[57] The trends for $S(t)$ in the "$I_2^+$" RMs reflect this increase in solvent mobility and demonstrate that the positively charged chromophore is a more sensitive probe of interfacial dynamics because of its localization there.

To gain additional insight into the differences in observed solvation dynamics, we decompose $S(t)$ into contributions from individual solvent species, according to eq 10. The results of this decomposition for the $w_0 = 4$ RM are depicted in Figure 4. In the case of the "$I_2^+$" solute, we omit from the plot $S_{Cl^-}(t)$ in view of its negligible contribution to $S(t)$.

It is evident that the three components of the RM interior play quite different roles in the response to charge localization in the two solutes. In the case of $I_2^-$, the headgroups do not contribute appreciably to solvation dynamics. After the fast initial response due mainly to water, $S_{H_2O}(t)$ and $S_{Na^+}(t)$ are of
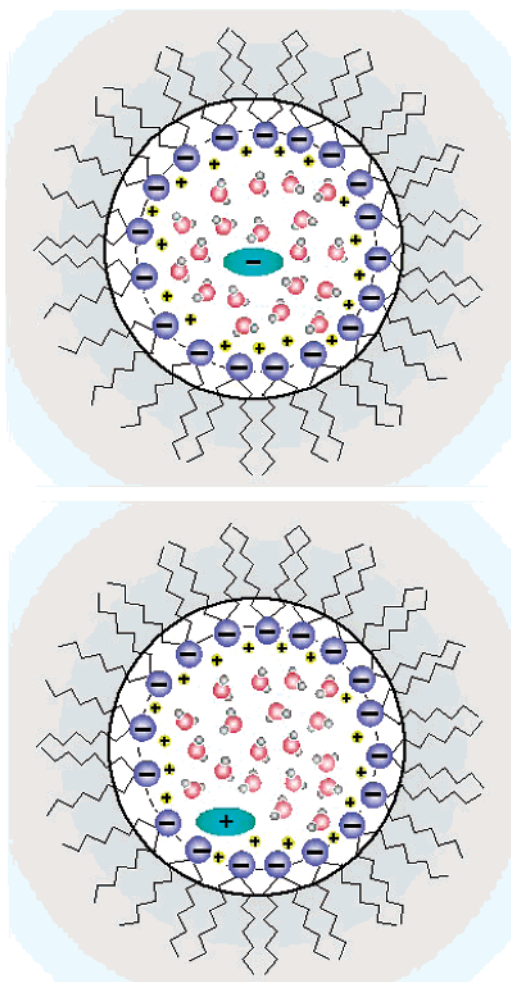
**Figure 2.** Schematic representation of the location of a solute that is repelled by the headgroups (top panel) and of a solute that is attracted to the headgroups (bottom panel).
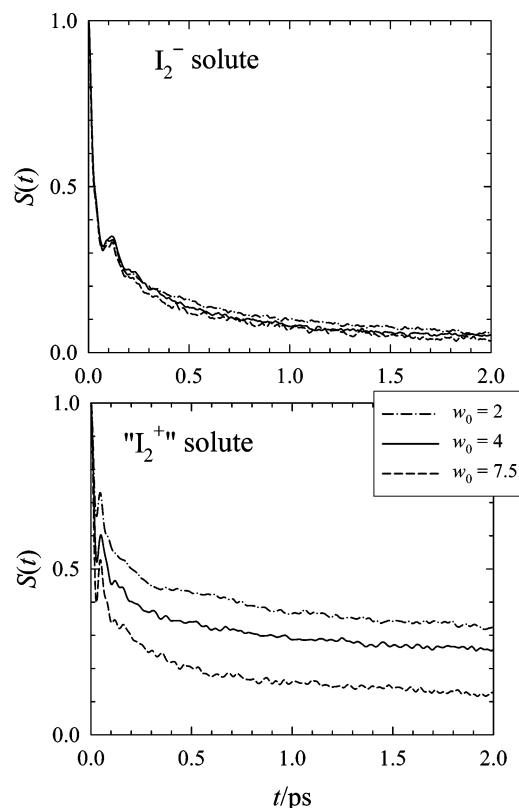


**Figure 3.** Nonequilibrium solvation response to charge localization in ionic solutes within anionic reverse micelles. The top panel depicts the results for $I_2^-$, and the bottom panel for "$I_2^+$". Different line styles represent the results for different $w_0$ values.

opposite signs, with the positive $S_{H_2O}(t)$ partially canceled by the negative $S_{Na^+}(t)$. In the case of "$I_2^+$", all three components contribute appreciably to $S(t)$ after the fast initial decay due to water reorientation. Because the headgroups have limited mobility, $S_{Z^-}(t)$ arises predominantly from the motion of the solute relative to the interface. In this case, $S_{Z^-}(t)$ is negative while $S_{H_2O}(t)$ and $S_{Na^+}(t)$ are positive. At longer times, $S_{Z^-}(t)$ and $S_{Na^+}(t)$ nearly cancel each other, leading to long-time decay similar to that of $S_{H_2O}(t)$.

Table 4 lists the contributions from all the solvent components to the steady-state fluorescence Stokes shift for the "$I_2^+$" solute. Specifically, the table entry for component $m$ corresponds to

$$\Delta\tilde{\nu}_m = \frac{\overline{\Delta E_m(0)} - \overline{\Delta E_m(\infty)}}{hc} \qquad (11)$$

and the total Stokes shift $\Delta\tilde{\nu}$ corresponds to the sum over $m$ of the component contributions, $\Delta\tilde{\nu}_m$. The analogous decomposition $\Delta\tilde{\nu}$ for the $I_2^-$ solute was reported in Table 4 of ref 56. As noted earlier, our model chromophores are smaller than the probes used in solvation dynamics experiments, and the change in solute dipole magnitude resulting from the $S_0 \rightarrow S_1$ transition is about three 3 larger than that for C343, the commonly used experimental probe of aqueous solvation dynamics. Thus the value of $\Delta\tilde{\nu}$ is about an order of magnitude higher.

The data in Table 4 show that the total $\Delta\tilde{\nu}$ is weakly dependent on $w_0$ but that the contributions from the three major

solvent components ($H_2O$, $Na^+$, and $Z^-$) vary with $w_0$. The headgroups and counterions play considerably larger roles in the smallest RM, $w_0 = 2$, where their contributions are almost as large in magnitude as the contribution of water. In the two larger RMs, their contributions diminish but are still appreciable. As could have been anticipated from Figure 4, the headgroup and counterion contributions are of opposite signs, which leads to their partial cancellation.

Except for the fact that the overall $\Delta\tilde{\nu}$ is weakly dependent on $w_0$, the steady-state Stokes shift results for $I_2^-$ are quite different. In that case, the headgroup contribution is negligible, and the water and $Na^+$ contributions are both positive, adding constructively to produce the total shift.

**C. Solute Location Change and Longer-Time Solvation Dynamics.** The results of Figure 4, which shows that $S_{Z^-}(t)$ contributes significantly to longer-time solvation dynamics, suggest that solute motion relative to the interface plays an important role in the diffusive portion of $S(t)$ decay for the "$I_2^+$" solute. We explore here the change in the solute location and the solvation time scale associated with this process.

Figure 5 depicts the iodine atom probability distribution for the equilibrated ground- and excited-state solutes as well as the nonequilibrium distribution at 5 ps after excitation. As can be seen from the figure, in all cases the distribution at 5 ps resembles more strongly the ground- than the excited-state distribution. Greatest progress toward reaching the excited-state equilibrium distribution is seen in the case of $w_0 = 7.5$, consistent with the fact that the interfacial solvent mobility increases with $w_0$.

Figure 5 also shows that the solute is, on average, further away from the interface in the $S_1$ than in the $S_0$ state. The equilibrium distribution for the $S_1$ state solute exhibits a single

Solvation Dynamics in Reverse Micelles

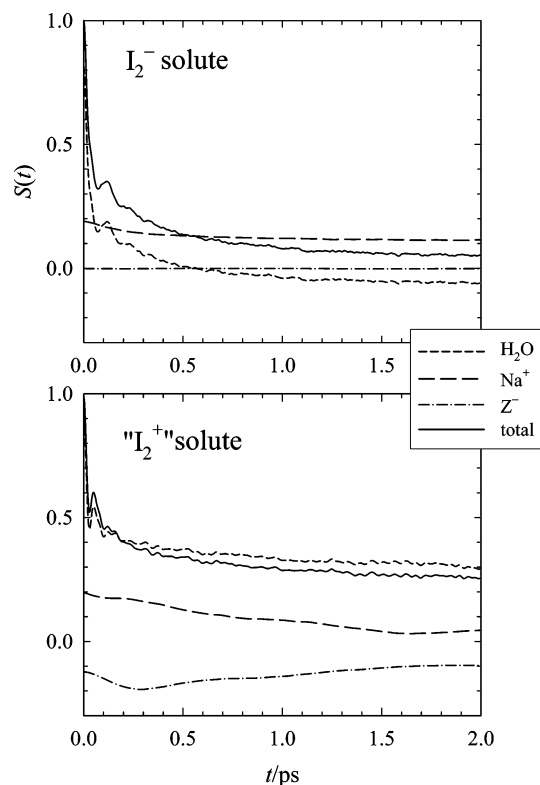*J. Phys. Chem. B, Vol. 109, No. 14, 2005* **6737**



**Figure 4.** Decomposition of the nonequilibrium solvation response, $S(t)$, into responses from the components of the RM interior, $H_2O$, $Na^+$ counterions, and the headgroups, $Z^-$, for $w_0 = 4$. The results for the $I_2^-$ solute are depicted in the top panel, and results for "$I_2^+$" in the bottom panel.

**TABLE 4: Steady-State Stokes Shifts (in $10^4$ cm$^{-1}$) for "$I_2^+$" in Reverse Micelles**

| $w_0$ | $\Delta\tilde{\nu}_{H_2O}$ | $\Delta\tilde{\nu}_{Na^+}$ | $\Delta\tilde{\nu}_{Z^-}$ | $\Delta\tilde{\nu}_{Cl^-}$ | $\Delta\tilde{\nu}_{total}$ |
|---|---|---|---|---|---|
| 2 | 2.25 | 2.66 | −1.84 | −0.08 | 2.99 |
| 4 | 2.62 | 0.59 | −0.37 | 0.02 | 2.86 |
| 7.5 | 2.47 | 0.67 | −0.21 | −0.03 | 2.90 |

peak located at about 5 Å from the headgroup positions. This peak overlaps the third diffuse peak in the $S_0$ distribution and corresponds to a radial location close to contact with the interior surface of the headgroups. Thus, in the excited state, the solute is no longer embedded in the interface but has moved to the border of the interfacial and core regions.

Unlike in the ground state, for which the two "$I_2^+$" solute atoms carry equivalent $0.5e$ charges, the charge in the excited-state solute is localized on one of the atoms. Thus, for the excited state, we do not expect the location of the two solute atoms to be equivalent. In Figure 5, we displayed the distribution that corresponds to the sum of the $I^+$ and $I^0$ excited-state distributions. In Figure 6, we show the individual solute atom distributions in addition to their sum.

There is a clear evolution in the $I^+$ and $I^0$ distributions as $w_0$ increases. In the smallest RM, they are well-separated, with the sharper $I^+$ distribution closer to the headgroup location. As $w_0$ increases, the distance between the two peaks diminishes. The distributions also broaden, with the extent of broadening more dramatic for $I^+$ than for $I^0$. The result is that in the $w_0 = 7.5$ RM the peaks of the two distributions essentially coincide and the $I^+$ distribution is broader than the $I^0$ distribution. This trend is likely to be related to the fact that the surface area per headgroup increases with $w_0$, allowing for a wider range of solute locations that satisfy the Coulomb attraction between the
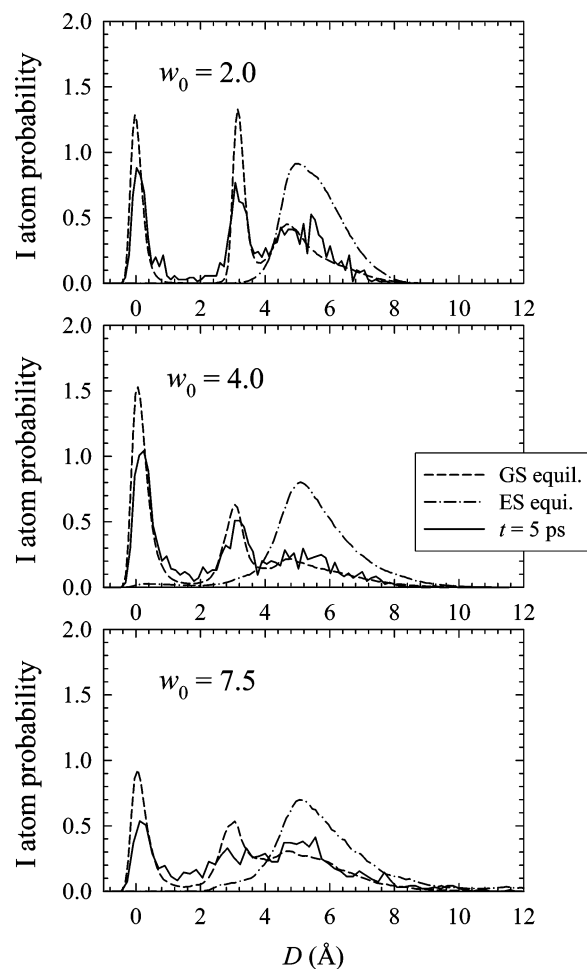


**Figure 5.** The time evolution of the "$I_2^+$" solute location after electronic excitation resulting in solute charge localization. Different line styles depict the results for $t = 0$ (equilibrium delocalized charge distribution), $t = 5$ ps after excitation, and $t = \infty$ (equilibrium localized charge distribution). The results in the top, middle, and bottom panels are, respectively, for $w_0 = 2$, 4, and 7.5.

headgroup and the $I^+$ site and that accommodate the hydrophobic $I^0$ site.

Figures 5 and 6 indicate that the change in the "$I_2^+$" solute location upon electronic excitation is weakly dependent on $w_0$. Thus it is likely that it is the local viscosity of the solvent through which the solute moves to reach its final location that determines the time scale of the slowly decaying portion of $S(t)$ for charge localization in this solute.

Figure 7 focuses on this solvation time scale by showing a semilog plot of $S(t)$ for $0 \leq t \leq 5$ ps in all three RM sizes. Also shown are fits of the longer-time ($t > 0.4$ ps) decay of $S(t)$ to a sum of two exponentials

$$S(t > 0.4\text{ ps}) \cong F(t) = a_1 e^{-t/\tau_1} + a_2 e^{-t/\tau_2} \quad (12)$$

The fitted parameters are reported in Table 5. The smaller of the two times, $\tau_1$, fits the shorter-time decay rate of $S(t)$ only moderately well. It decreases from about 0.8 to about 0.5 ps in going from $w_0 = 2$ to 4, but then does not change significantly as $w_0$ increases further. The fit to eq 12 becomes excellent at longer times, so it seems reasonable to place greater weight on the significance of the parameters associated with this decay process. Both $a_2$ and $\tau_2$ decrease with increasing $w_0$, but even for the largest RM $\tau_2$ exceeds the depicted time interval by a factor of 2. Our studies of the water mobility near the RM
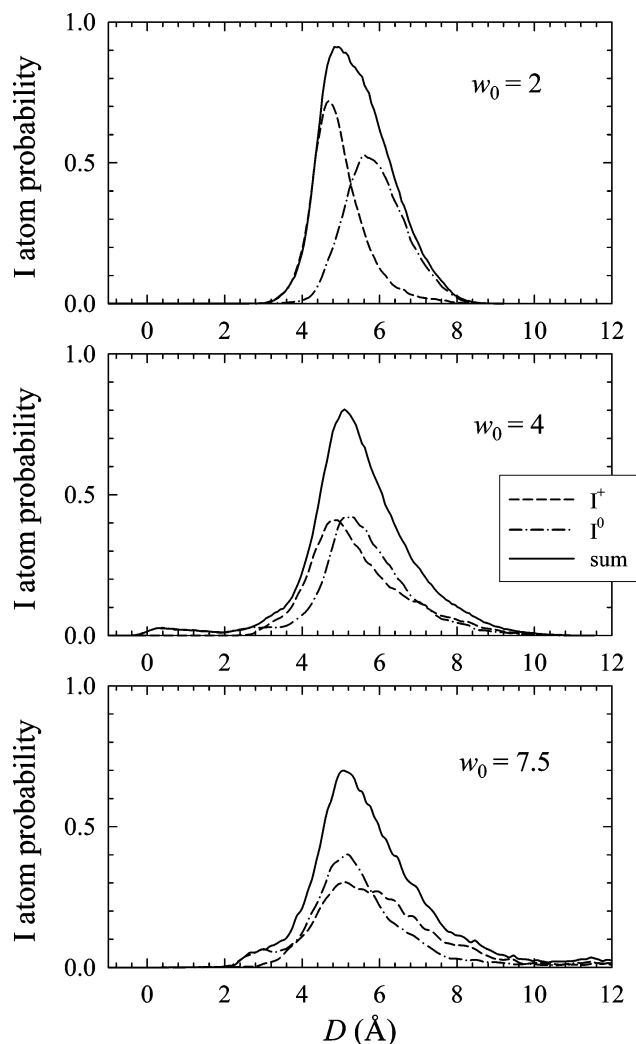
**Figure 6.** Solute site probability densities for the excited-state "$I_2^+$" in RMs of different size as functions of $D$, the distance from the average headgroup location. The top, middle, and bottom panels depict, respectively, the results for $w_0 = 2$, 4, and 7.5. Different line styles correspond to the probabilitiy densities for $I^+$, $I^0$, and their sum.

interface indicate that it is more strongly suppressed in smaller reverse micelles.[57,70] Thus, we would expect that the solute diffusing through this region would experience a more viscous solvent environment in smaller than in larger RMs. The RM size dependence of the time $\tau_2$ is consistent with this expectation.

Given that the change in solute location is weakly dependent on $w_0$, we ascribe the decrease in $a_2$ with increasing $w_0$ mainly to the decreasing relative importance of the contributions of headgroups and counterions to $S(t)$ in larger reverse micelles. This expectation, which is confirmed in part by the $\Delta\tilde{\nu}$ results in Table 4, is based on the fact that the interfacial density of the surfactant headgroups and the $Na^+$ ions diminishes with increasing $w_0$.[32,57]

**D. Nonlinear Aspects of the Solvation Response.** In bulk water, the solvation response associated with changes in the solute−solvent electrostatic interactions is often close to linear,[82−87] with $S(t)$ resembling a solvation time correlation of $\delta\Delta E$ in the presence of either the ground- ($C_0(t)$) or the excited ($C_1(t)$)-state solute (eq 7). We found that for the charge localization in $I_2^-$ in AOT-like reverse micelles the approximation $S(t) \cong C_0(t)$ is quite good and that its accuracy was weakly correlated with $w_0$.[56] In Figure 8, we carry out this
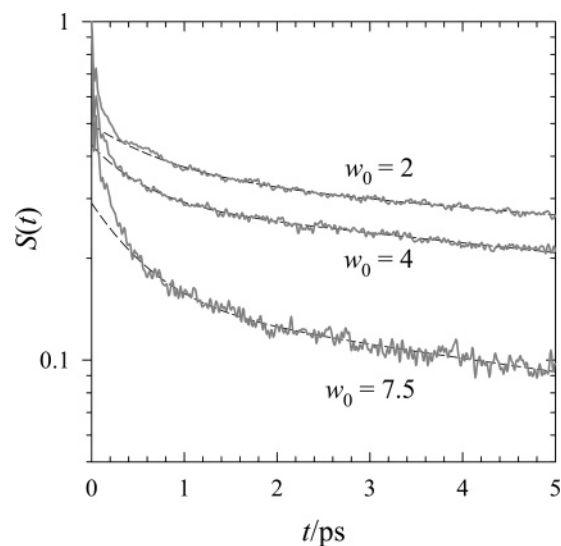


**Figure 7.** Nonequilibrium solvation responses for the "$I_2^+$" solute in RMs of different size. The full lines represent the MD simulation results, and the dashed lines a fit of the longer-time ($t > 0.4$ ps) response to biexponential decay.

**TABLE 5: Fit of Longer-Time Solvation Response for "$I_2^+$" to Biexponential Decay**

| $w_0$ | $a_1$ | $\tau_1$ (ps) | $a_2$ | $\tau_2$ (ps) |
|---|---|---|---|---|
| 2 | 0.153 | 0.826 | 0.343 | 20.2 |
| 4 | 0.142 | 0.528 | 0.290 | 15.0 |
| 7.5 | 0.146 | 0.560 | 0.146 | 10.9 |

comparison for "$I_2^+$" in RMs with $w_0 = 2$ and 7.5. The results for $w_0 = 4$, which are not displayed, are intermediate between these two.

We see that in this case $C_0(t)$ and $S(t)$ agree reasonably well on the inertial and librational time scales ($t < 0.1$ ps) but that at longer times $C_0(t)$ decays considerably faster than $S(t)$. The disagreement between the nonlinear and linear solvation response is larger for the smaller RM. This result is consistent with the fact that the change in the solute location relative to the interface plays an important role in the longer-time solvation dynamics and that the contribution to $S(t)$ from nonaqueous species is larger on this time scale for the solute in the smaller RM. $C_0(t)$, which samples fluctuations in $\Delta E$ at the initial solute location, is unable to capture the dynamics associated with the excited-state solute location change.

**V. Summary and Conclusions**

We have presented computer simulation results on solvation dynamics of anionic and cationic chromophores in model anionic-surfactant RMs designed to represent water/AOT/oil. The RM water content $w_0$ was varied from 2 to 7.5. As we had shown earlier for this RM model, water mobility throughout the droplet is affected by the presence of the interface in this range of $w_0$. The mobility is suppressed more strongly in the vicinity of the interface due to interactions of water with the headgroups and $Na^+$ counterions. In all RM regions, the mobility increases with increasing $w_0$ due in part to an accompanying increase in the surface area per headgroup.

We find dramatic differences in solvation dynamics results for ionic chromophores that differ only in charge sign. The negatively charged chromophore, modeled as a rigid $I_2^-$, exhibits weak dependence of $S(t)$ on RM size and a fast decay rate, similar to the time scale found in bulk water. It also exhibits a negligible contribution from the surfactant headgroups. These
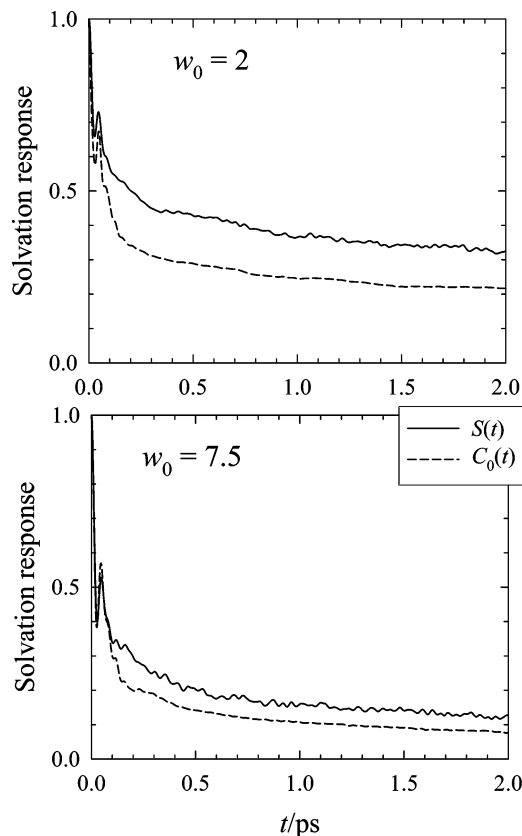
Solvation Dynamics in Reverse Micelles

*J. Phys. Chem. B, Vol. 109, No. 14, 2005* **6739**



**Figure 8.** Comparison of the nonequilibrium solvation response $S(t)$ and the ground-state solvation TCF $C_0(t)$ for the "$I_2^+$" solute in RMs of different size. The results for $w_0 = 2$ are shown in the top panel, and those for $w_0 = 7.5$ in the bottom panel.

observations are consistent with the fact that $I_2^-$ is not in the vicinity of the interface.

Solvation dynamics for a positively charged, but otherwise identical chromophore, "$I_2^+$", by contrast shows a strong dependence on $w_0$, with $S(t)$ decay markedly slower in $w_0 = 2$ than that in $w_0 = 7.5$. In all RM sizes we considered, $S(t)$ for "$I_2^+$" decays considerably more slowly than for $I_2^-$. The interaction of "$I_2^+$" with the surfactant headgroups is a significant contributor to the longer-time decay of $S(t)$.

We showed that the slow decay of $S(t)$ for the cationic chromophore has two main causes. The first is its initial location, partially embedded in the interface, the region of lowest solvent mobility.[57] The second is the fact that the solute's final location is significantly different, requiring that the solute move relative to the interface. The solute motion is on a significantly longer time scale than the collective reorientation of water molecules, contributing to the slowly decaying portion of $S(t)$. We note that the large-amplitude motion of the solute arises in part due to the large perturbation in its charge distribution. It remains to be seen to how much solute motion will contribute in the case of large organic probe molecules typically used in experiments. Given the larger size of these chromophores, the solute motion is likely to be on an even slower time scale than found in the present simulation. For example, in a recent simulation of solvation dynamics of C343 at the water/zirconia interface,[27] the contribution of solute reorientation was found to be on the nanosecond time scale.

This study illustrates the important roles of solute interactions with different phases and of the solute motion relative to the interface in $\Delta E$ relaxation in heterogeneous environments. We found that solute motion can contribute substantially to $S(t)$ even

when the chromophore is restricted to the RM aqueous phase. One can envisage even more extensive changes in location for chromophores, initially in the nonpolar phase, moving to the RM interior as their polarity increases on electronic excitation. Given the possibility of such events, one needs to expand the interpretation of $S(t)$ from the measure of local solvent reorganization to a measure of the change in the local solute environment, which can occur through solute as well as solvent motions.

**References and Notes**

(1) Reichardt, C. *Solvents and Solvent Effects in Organic Chemistry*, 2nd ed.; VCH: New York, 1988.
(2) Bagchi, B. *Annu. Rev. Phys. Chem.* **1989**, *40*, 115.
(3) Barbara, P. F.; Jarzeba, W. *Adv. Photochem.* **1990**, *15*, 1.
(4) Simon, J. D. *Pure Appl. Chem.* **1990**, *62*, 2243.
(5) Maroncelli, M. *J. Mol. Liq.* **1993**, *57*, 1.
(6) Rossky, P. J.; Simon, J. D. *Nature* **1994**, *370*, 263.
(7) Stratt, R. M.; Maroncelli, M. *J. Phys. Chem.* **1996**, *100*, 12981.
(8) Maroncelli, M.; Kumar, V. P.; Papazyan, A. *J. Phys. Chem.* **1993**, *97*, 13.
(9) Ladanyi, B. M.; Stratt, R. M. *J. Phys. Chem.* **1995**, *99*, 2502.
(10) Ladanyi, B. M.; Maroncelli, M. *J. Chem. Phys.* **1998**, *109*, 3204.
(11) Bagchi, B.; Chandra, A. *Adv. Chem. Phys.* **1991**, *80*, 1.
(12) Raineri, F. O.; Perng, B.-C.; Friedman, H. L. *Electrochim. Acta* **1997**, *42*, 2749.
(13) Song, X.; Chandler, D. *J. Chem. Phys.* **1998**, *108*, 2594.
(14) Huang, J.; Bright, F. V. *Appl. Spectrosc.* **1992**, *46*, 329.
(15) Datta, A.; Mandal, D.; Pal, S. K.; Bhattacharyya, K. *J. Phys. Chem. B* **1997**, *101*, 10221.
(16) Behera, G. B.; Mishra, B. K.; Behera, P. K.; Panda, M. *Adv. Colloid Interface Sci.* **1999**, *82*, 1.
(17) Pant, D.; Levinger, N. E. *J. Phys. Chem. B* **1999**, *103*, 7846.
(18) Bhattacharyya, K. *J. Fluoresc.* **2001**, *11*, 167.
(19) Benderskii, A. V.; Eisenthal, K. B. *J. Phys. Chem. B* **2001**, *105*, 6698.
(20) Shang, X. M.; Benderskii, A. V.; Eisenthal, K. B. *J. Phys. Chem. B* **2001**, *105*, 11578.
(21) Thompson, W. H. *J. Chem. Phys.* **2002**, *117*, 6618.
(22) Benjamin, I. *Prog. React. Kinet. Mech.* **2002**, *27*, 87.
(23) Vieceli, J.; Benjamin, I. *J. Phys. Chem. B* **2003**, *107*, 4801.
(24) Munson, C. A.; Baker, G. A.; Baker, S. N.; Bright, F. V. *Langmuir* **2004**, *20*, 1551.
(25) Shirota, H.; Tamoto, Y.; Segawa, H. *J. Phys. Chem. A* **2004**, *108*, 3244.
(26) Thompson, W. H. *J. Chem. Phys.* **2004**, *120*, 8125.
(27) Martins, L. R.; Skaf, M. S.; Ladanyi, B. M. *J. Phys. Chem. B* **2004**, *108*, 19687.
(28) Luisi, P. L.; Straub, B. E. *Reverse Micelles: Biological and Technological Relevance of Amphiphilic Structures in Apolar Media*; Plenum: New York, 1984.
(29) Luisi, P. L.; Giomini, M.; Pileni, M. P.; Robinson, B. H. *Biochim. Biophys. Acta* **1988**, *947*, 209.
(30) *Structure and Reactivity in Reverse Micelles*; Pileni, M. P., Ed.; Elsevier: Amsterdam, 1989; Vol. 65.
(31) Pileni, M. P. *J. Phys. Chem.* **1993**, *97*, 6961.
(32) Eicke, H. F.; Rehak, J. *Helv. Chim. Acta* **1976**, *59*, 2883.
(33) De, T.; Maitra, A. *Adv. Colloid Interface Sci.* **1995**, *59*, 95.
(34) Wong, M.; Thomas, J. K.; Gratzel, M. *J. Am. Chem. Soc.* **1976**, *98*, 2391.
(35) Zhang, J.; Bright, F. V. *J. Phys. Chem.* **1991**, *95*, 7900.
(36) Zhang, J.; Bright, F. V. *J. Phys. Chem.* **1992**, *96*, 9068.
(37) Zhang, J.; Bright, F. V. *J. Phys. Chem.* **1992**, *96*, 5633.
(38) Sarkar, N.; Das, K.; Datta, A.; Das, S.; Bhattacharyya, K. *J. Phys. Chem.* **1996**, *100*, 10523.
(39) Bhattacharyya, K.; Bagchi, B. *J. Phys. Chem. A* **2000**, *104*, 10603.
(40) Nandi, N.; Bhattacharyya, K.; Bagchi, B. *Chem. Rev.* **2000**, *100*, 2013.
(41) Dutta, P.; Sen, P.; Mukherjee, S.; Halder, A.; Bhattacharyya, K. *J. Phys. Chem. B* **2003**, *107*, 10815.
(42) Bhattacharyya, K.; Hara, K.; Kometani, N.; Uozu, Y.; Kajimoto, O. *Chem. Phys. Lett.* **2002**, *361*, 136.

(43) Levinger, N. E.; Riter, R. E.; Willard, D. M.; Pant, D. *Springer Ser. Chem. Phys.* **1998**, *63*, 553.

(44) Pant, D.; Riter, R. E.; Levinger, N. E. *J. Chem. Phys.* **1998**, *109*, 9995.

(45) Riter, R. E.; Undiks, E. P.; Levinger, N. E. *J. Am. Chem. Soc.* **1998**, *120*, 6062.

(46) Riter, R. E.; Willard, D. M.; Levinger, N. E. *J. Phys. Chem. B* **1998**, *102*, 2705.

(47) Willard, D. M.; Riter, R. E.; Levinger, N. E. *J. Am. Chem. Soc.* **1998**, *120*, 4151.

(48) Levinger, N. E. *Curr. Opin. Colloid Interface Sci.* **2000**, *5*, 118.

(49) Pant, D.; Levinger, N. E. *Langmuir* **2000**, *16*, 10123.

(50) Willard, D. M.; Levinger, N. E. *J. Phys. Chem. B* **2000**, *104*, 11075.

(51) Corbeil, E. M.; Levinger, N. E. *Langmuir* **2003**, *19*, 7264.

(52) Jimenez, R.; Fleming, G. R.; Kumar, P. V.; Maroncelli, M. *Nature* **1994**, *369*, 471.

(53) Vajda, S.; Jimenez, R.; Rosenthal, S. J.; Fidler, V.; Fleming, G. R.; Castner, E. W., Jr. *J. Chem. Soc., Faraday Trans.* **1995**, *91*, 867.

(54) Mandal, D.; Datta, A.; Pal, S. K.; Bhattacharyya, K. *J. Phys. Chem. B* **1998**, *102*, 9070.

(55) Wong, M.; Thomas, J. K.; Nowak, T. *J. Am. Chem. Soc.* **1977**, *99*, 4730.

(56) Faeder, J.; Ladanyi, B. M. *J. Phys. Chem. B* **2001**, *105*, 11148.

(57) Faeder, J.; Ladanyi, B. M. *J. Phys. Chem. B* **2000**, *104*, 1033.

(58) Allen, M. P.; Tildesley, D. J. *Computer Simulation of Liquids*; Clarendon: Oxford, 1987.

(59) Lee, C. Y.; McCammon, J. A.; Rossky, P. J. *J. Chem. Phys.* **1984**, *80*, 4448.

(60) Berendsen, H. J. C.; Grigera, J. R.; Straatsma, T. P. *J. Phys. Chem.* **1987**, *91*, 6269.

(61) Schweighofer, K. J.; Essmann, U.; Berkowitz, M. *J. Phys. Chem. B* **1997**, *101*, 3793.

(62) Griffiths, J. A.; Heyes, D. M. *Langmuir* **1996**, *12*, 2418.

(63) Salaniwal, S.; Cui, S. T.; Cochran, H. D.; Cummings, P. T. *Langmuir* **2001**, *17*, 1773.

(64) Salaniwal, S.; Cui, S. T.; Cochran, H. D.; Cummings, P. T. *Langmuir* **2001**, *17*, 1784.

(65) Tobias, D. J.; Klein, M. L. *J. Phys. Chem.* **1996**, *100*, 6637.

(66) Senapati, S.; Berkowitz, M. L. *J. Chem. Phys.* **2003**, *118*, 1937.

(67) Senapati, S.; Berkowitz, M. L. *J. Phys. Chem. B* **2003**, *107*, 12906.

(68) Abel, S.; Sterpone, F.; Bandyopadhyay, S.; Marchi, M. *J. Phys. Chem. B* **2004**, *108*, 19458.

(69) Pandit, S. A.; Bostick, D.; Berkowitz, M. L. *J. Chem. Phys.* **2003**, *119*, 2199.

(70) Harpham, M. R.; Ladanyi, B. M.; Levinger, N. E.; Herwig, K. W. *J. Chem. Phys.* **2004**, *121*, 7855.

(71) Benjamin, I.; Whitnell, R. M. *Chem. Phys. Lett.* **1993**, *204*, 45.

(72) Cave, R. J.; Castner, E. W. *J. Phys. Chem. A* **2002**, *106*, 12117.

(73) Dang, L. X. *Chem. Phys. Lett.* **1994**, *227*, 211.

(74) Ciccotti, G.; Ryckaert, J.-P. *Comput. Phys. Rep.* **1986**, *4*, 345.

(75) Berendsen, H. J. C.; Postma, J. P. M.; van Gunsteren, W. F.; DiNola, A.; Haak, J. R. *J. Chem. Phys.* **1984**, *81*, 3684.

(76) Carter, E. A.; Hynes, J. T. *J. Chem. Phys.* **1991**, *94*, 5961.

(77) Stephens, M. D.; Saven, J. G.; Skinner, J. L. *J. Chem. Phys.* **1997**, *106*, 2129.

(78) Tran, V.; Schwartz, B. J. *J. Phys. Chem. B* **1999**, *103*, 5570.

(79) Horng, M. L.; Gardecki, J. A.; Papazyan, A.; Maroncelli, M. *J. Phys. Chem.* **1995**, *99*, 17311.

(80) Geissler, P. L.; Chandler, D. *J. Chem. Phys.* **2000**, *113*, 9759.

(81) Hansen, J. P.; McDonald, I. R. *Theory of Simple Liquids*, 2nd ed.; Academic Press: London, 1986.

(82) Maroncelli, M.; Fleming, G. R. *J. Chem. Phys.* **1988**, *89*, 5044.

(83) Bader, J. S.; Chandler, D. *Chem. Phys. Lett.* **1989**, *157*, 501.

(84) Levy, R. M.; Kitchen, D. B.; Blair, J. T.; Krogh-Jespersen, K. *J. Phys. Chem.* **1990**, *94*, 4470.

(85) Ando, K.; Kato, S. *J. Chem. Phys.* **1991**, *95*, 5966.

(86) Muiño, P. L.; Callis, P. R. *J. Chem. Phys.* **1994**, *100*, 4093.

(87) Ladanyi, B. M.; Skaf, M. S. *Annu. Rev. Phys. Chem.* **1993**, *44*, 335.